

Suppression of Bragg reflection glitches of a single-crystal diamond anvil cell by a polycapillary half-lens in high-pressure XAFS spectroscopy

Dongliang Chen,^{a*} Juncai Dong,^a Xiaoli Zhang,^a Peiyu Quan,^a Yaxiang Liang,^a Tiandou Hu,^a Jing Liu,^a Xiang Wu,^{b*} Qian Zhang^b and Yude Li^c

^aBeijing Synchrotron Radiation Facility, Institute of High Energy Physics, Chinese Academy of Sciences, Beijing 100049, People's Republic of China, ^bKey Laboratory of Orogenic Belts and Crustal Evolution, MOE, Peking University, and School of Earth and Space Sciences, Peking University, Beijing 100871, People's Republic of China, and ^cLaboratory for X-ray Optics, College of Nuclear Science and Technology, Beijing Normal University, Beijing 230029, People's Republic of China. E-mail: chendl@ihep.ac.cn, xiang.wu@pku.edu.cn

In combination with a single-crystal diamond anvil cell (DAC), a polycapillary half-lens (PHL) re-focusing optics has been used to perform high-pressure extended X-ray absorption fine-structure measurements. It is found that a large divergent X-ray beam induced by the PHL leads the Bragg glitches from single-crystal diamond to be broadened significantly and the intensity of the glitches to be reduced strongly so that most of the DAC glitches are efficiently suppressed. The remaining glitches can be easily removed by rotating the DAC by a few degrees with respect to the X-ray beam. Accurate X-ray absorption fine-structure (XAFS) spectra of polycrystalline Ge powder with a glitch-free energy range from -200 to 800 eV relative to the Ge absorption edge are obtained using this method at high pressures up to 23.7 GPa, demonstrating the capability of PHL optics in eliminating the DAC glitches for high-pressure XAFS experiments. This approach brings new possibilities to perform XAFS measurements using a DAC up to ultrahigh pressures.

Keywords: high-pressure μ -XAFS; DAC; polycapillary half-lens optics; Ge K-edge.

1. Introduction

X-ray absorption fine-structure (XAFS) spectroscopy, including the X-ray absorption near-edge structure (XANES) spectroscopy and extended X-ray absorption fine-structure (EXAFS) spectroscopy, has been proved to be a powerful technique for probing both local atomic and electronic structures around a selected atom of materials (Bunker, 2010). XAFS studies can be performed not only on crystals but also on materials without long-range order, including amorphous systems, glasses, quasicrystals, solutions, liquids and gas at ambient or extreme conditions, such as high/low temperature, high pressure, *etc.* (Koningsberger & Prins, 1987; Itié *et al.*, 1992). Diamond anvil cells (DACs) are currently the most widely used of all high-pressure devices, which can introduce the fundamental thermodynamic variable of pressure to explore the high-pressure behavior of materials. This is mainly due to merits such as the hardness of diamond which can push the highest achievable pressures to the megabar region, and transparency in a broad spectral range covering X-rays (typically above 5 keV) to infrared light (Jayaraman, 1983; Itié *et al.*, 2005). The combination of DACs and XAFS has long

been regarded as a very important technique for investigating the high-pressure behavior and evolution of the local atomic and electronic structure of materials, becoming a standard experimental set-up for studying materials at high pressure. However, a pair of diamond anvils with typical thickness of 4 – 4.5 mm is not only opaque to the low-energy absorption edges but also produces several Bragg glitches riding on the XAFS spectrum. The Bragg glitches are often more intensive than the EXAFS and XANES oscillations, resulting in damage to the high-quality EXAFS necessary for deriving quantitative structural information. Therefore, the application of XAFS spectroscopy as a quantitative local structural characterization technique is severely limited in high-pressure physics.

The number of Bragg glitches in a given energy range is roughly proportional to the square of the edge energy. Besides, the energy positions and intensities of these glitches are extremely sensitive to the photon energy and the orientation of the single-crystal diamonds relative to the incident X-ray beam (Pascarelli *et al.*, 2004; Hong *et al.*, 2009). Accordingly, one often measures the XAFS spectra at several different orientations of the DAC since each rotation moves the glitches to new positions. By observing the changes of

position of the Bragg glitches and searching for an optimum orientation, the glitches can be moved out of the region of interest by DAC rotation, and then it is, in general, possible to eliminate all Bragg glitches over the whole energy range of an XAFS spectrum (Itié *et al.*, 2005; Hong *et al.*, 2009). Even so, the practice of performing measurements at an optimum DAC orientation is quite tricky and rather time-consuming. Energy-dispersive XAFS has proven to be more effective than energy-scanning XAFS for addressing such a challenge (Pascarelli *et al.*, 2004; Hong *et al.*, 2009; Baldini *et al.*, 2010). This method, performed at low energies (for Ni, Cu *K*-edges), seems to be able to make the glitch-free energy window wide enough (Sapelkin *et al.*, 2000; Vanpeteghem *et al.*, 2001; Itié *et al.*, 2005), but it is almost impossible to obtain a glitch-free XAFS spectrum for those absorption edges with higher energies. For example, so far the largest possible glitch-free energy range for the Ge *K*-edge XAFS spectrum can be reached at about 440 eV above the Ge *K*-edge, resulting in the upper limit of the *k*-range of the EXAFS signal extending to only a maximum of 7–8 Å⁻¹ (Itié *et al.*, 2005; Hong *et al.*, 2009; Baldini *et al.*, 2010). Hence, such an EXAFS signal with a short *k*-range cannot be used for the accurate structural determination of higher coordination shells owing to a limited number of free parameters, severely prohibiting the exploitation of EXAFS in high-pressure physics (Jayaraman, 1983; Hong *et al.*, 2009; Baldini *et al.*, 2010, 2011).

In fact, several methods to avoid DAC glitches for XAFS measurements at high pressures have been reported over the years, such as the use of sapphire (Tamura *et al.*, 1992) and polycrystalline boron carbide (B₄C) anvils (Tolbert & Alivisatos, 1995), multi-anvil presses (Katayama *et al.*, 1996) or a large-volume Paris–Edinburgh press (Katayama *et al.*, 1997). Unfortunately the maximum achievable pressure for these devices is strongly limited compared with DACs. More recently, a DAC with nanocrystalline diamond anvils has been employed in a high-pressure glitch-free EXAFS experiment, showing evident advantages for coupling EXAFS and DAC techniques (Baldini *et al.*, 2011). Another effective way for eliminating the diamond glitches is to use an iterative algorithm based on repeated XAFS measurements over a small angular range of DAC orientation relative to the X-ray beam direction (Hong *et al.*, 2009). Nonetheless, the practice of this approach is quite tricky and the data need to be further processed quite carefully.

In the following, we adopt a different methodological strategy to avoid DAC glitches for XAFS measurements at high pressures. The approach is based on the traditional single-crystal diamond anvils, classical energy-scanning XAFS mode and microfocusing optics at beamline 4W1B of Beijing Synchrotron Radiation Facility (BSRF), China. The main feature of our method is the microfocusing optical system, which consists of a toroidal mirror and a polycapillary half-lens (PHL). With appropriate pre-focusing by the toroidal mirror, the PHL can be an effective re-focusing device for producing microbeams with high flux density and large angular divergence. We find that the large angular divergence induced by the PHL optics opens up the possibility to avoid

DAC glitches for high-pressure XAFS. For X-ray diffraction experiments, it is well known that the Bragg reflection peaks become more and more broadened with increasing angular divergence of the X-ray beam. Therefore, a large divergent X-ray beam induced by the PHL can lead the Bragg peaks of single-crystal diamond to be broadened substantially and the intensity of Bragg peaks to be strongly reduced so that the Bragg glitches are possibly suppressed, whereas the XAFS spectrum cannot be affected by the divergence.

We explore the capabilities of our optical system to avoid DAC glitches for μ -EXAFS measurements at high pressure in transmission mode. Demonstrative XAFS spectra of polycrystalline Ge powder were collected at beamline 4W1B using our method at high pressures up to 23.7 GPa, showing no DAC glitches up to 800 eV above the absorption edge of Ge. Although the PHL has been used with DACs already in a number of studies of X-ray fluorescence (XRF) analysis (Schmidt *et al.*, 2006; Wilke *et al.*, 2010; Petitgirard *et al.*, 2012), and the use of PHLs in μ -EXAFS for both fluorescence and transmission modes has also been demonstrated (Vincze *et al.*, 2002; Proost *et al.*, 2003; Silversmit *et al.*, 2009), the detailed characterization of the use of PHL optics in high-pressure μ -EXAFS with a single-crystal DAC has, to the best of our knowledge, not yet been reported. Considering that beamline 4W1B's microprobe program is mainly devoted to micrometer-scale XRF mapping and μ -EXAFS with fluorescence mode for samples with proper structural size, this approach allowed us to extend our optical system to apply for high-pressure XAFS measurements using a DAC.

2. Experimental

Beamline 4W1B is located at a single-period wiggler source of BSRF, where the storage ring is run with electrons at an energy of 2.5 GeV and 150–250 mA ring current. The horizontal and vertical angular acceptance of the source are 1.3 mrad and 0.17 mrad, respectively, and its size is 2.4 mm (H) \times 0.312 mm (V). The optical layout consists of a front slit and a fixed-exit Si(111) double-crystal monochromator, followed by a rhodium-coated toroidal mirror and by a PHL positioned just before the sample. The water-cooled Si(111) double-crystal monochromator, located 17.99 m downstream of the source, covers the energy range 4.5–22 keV. A toroidal mirror with an optical length of 1 m, located 19.28 m downstream from the source, follows the monochromator and pre-focuses the monochromatic beam in both of the horizontal and vertical directions at the focal point, located at 23.9 m downstream of the source. The water-cooled toroidal mirror receives the beam at 3.6 mrad. The mirror cut-off is, at this angle, approximately 18.6 keV. The mirror is capable of providing a focus of 0.67 mm (H) and 0.62 mm (V) FWHM with a photon flux of 6×10^{10} photons mm⁻² s⁻¹ at 10 keV.

Re-focusing is achieved using a large-acceptance PHL with an entrance diameter of 20 mm, an optical length of 50 mm and an exit diameter of 7 mm, manufactured by Beijing Normal University of China and specifically designed for the beam characteristics of 4W1B. The holder of the PHL is

mounted on an $xy\theta\varphi$ positioner including translational, rotary and tilt stages, which could provide all the necessary degrees of freedom for alignment of the PHL. The PHL focusing optics has a focus depth of about 300 μm . A spot size of 65 μm FWHM and PHL tip-to-focus distance of 21 mm are measured for the focused beam at 10 keV, meaning that the sample would need to be placed 21 mm away from the tip of the PHL. The exit-angle divergence from the PHL optics can therefore be estimated to be about 15 mrad. The beam size decreases as a function of increasing X-ray energy, and is between 48 and 74 μm in the 7–15 keV energy range with a transmission efficiency of 37–21%.

The combined micro-optics configuration of the toroidal mirror and PHL are used in energy-scanning μ -EXAFS (μ -XANES and μ -EXAFS) for both fluorescence and transmission modes at beamline 4W1B. For the transmission μ -EXAFS, two AXUV36 Si photodiodes manufactured by IRD (International Radiation Detectors, <http://www.ird-inc.com/index.html>), which consist of a Si chip of thickness 5 μm , substitute for ion chambers and are used to measure the flux of the incoming and transmitted microbeam, since the PHL tip-to-focus distance (21 mm) is very limited and the beam diverges rapidly from the tip of the PHL. As displayed in Fig. 1, the first Si photodiode (SPD) is placed between the DAC and PHL, and kept as close as possible to the tip of the PHL. The DAC holder is fixed upon a $xyz\theta\varphi$ stage. The three translations and two rotations stage, with its origin at the exit of the PHL optics, the x -axis in the horizontal plane defined by the

synchrotron orbit, the y -axis in the vertical direction, the z -axis along the X-ray beam propagation, the θ rotation around the y -axis and the φ rotation around the z -axis, is used for optimizing the position and orientation of the DAC simultaneously. A second SPD is located downstream of the DAC holder to monitor the microbeam.

In the present high-pressure experiments, a piston-type DAC designed by Bayerisches Geoinstitut, Germany, was employed for XAFS measurements. The pair of anvils is of thickness 4.4 mm with 300 μm -diameter culets. A hole of approximately 100 μm in diameter was drilled in the center as the sample chamber in the pre-indented 40 μm rhenium gasket. Owing to its softness and lower X-ray absorption properties, LiF was used as the pressure-transmitting medium. The thickness of polycrystalline Ge powder with 99.999% purity (Sigma-Aldrich) was about 14.2 μm in order to guarantee that the edge jump of Ge is around unity during the compression process. One small ruby sphere was loaded into the corner of the sample chamber for pressure calibration according to its R1 fluorescence peak position. The measurements were performed up to 23.7 GPa. The high-pressure XAFS spectra of polycrystalline Ge powder were collected by scanning the energy from -200 to 800 eV. The XAFS data were analyzed using *IFEFFIT* (Ravel & Newville, 2005).

3. Results and discussion

A comparison with the well established transmission-mode XAFS method by using ion chambers would be a strict criterion for our method by using Si photodiodes to monitor the X-ray beam, and to ensure that the XAFS spectrum is not distorted by the Si photodiode. The transmission Ge K -edge XAS spectra of polycrystalline Ge powder are recorded under ambient conditions with Si photodiodes and ion chambers, respectively, and then are background-subtracted, normalized and plotted in Fig. 2(a) for comparison. No obvious discrepancy has been observed. Figs. 2(b) and 2(c) show the k^2 -weighted $\chi(k)$ functions and their Fourier transforms, respectively. The excellent consistency has demonstrated that high-quality transmission XAFS spectra can be obtained using Si photodiodes to measure both the incident and transmission X-ray flux. In addition, the Bragg reflection glitches caused by the Si single crystal of Si photodiode itself are not observed in this energy range. It is obvious that the PHL optical system certainly plays an important role in avoiding the Bragg peaks of silicon. Recently, Krumrey *et al.* have reported a transmission performance comparison among several different Si photodiodes (Krumrey *et al.*, 2007). Their results show that thin photodiodes are well suited as transmission intensity detectors for hard X-rays with photon energy above ~ 4 keV, but their responsivity and transmittance depend critically on the thickness and homogeneity of the Si chips, which should be further improved by the manufacturers.

In order to examine the performance of our PHL optics on suppression of DAC glitches, we have measured four Ge K -edge XAFS spectra of polycrystalline Ge powder using a

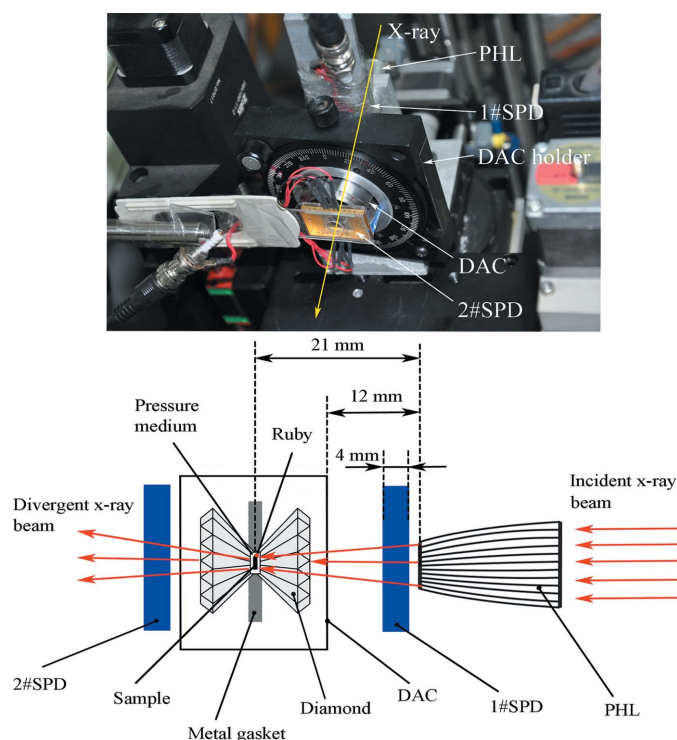


Figure 1
Top: photograph showing the top view of the experimental set-up at beamline 4W1B. Downstream of the PHL tip is the 1#SPD. The DAC is mounted on a holder which is on a motorized $xyz\theta\varphi$ stage, followed by the 2#SPD. Bottom: schematic illustration showing a side view of the detailed geometry of the high-pressure XAFS experimental set-up with a DAC.

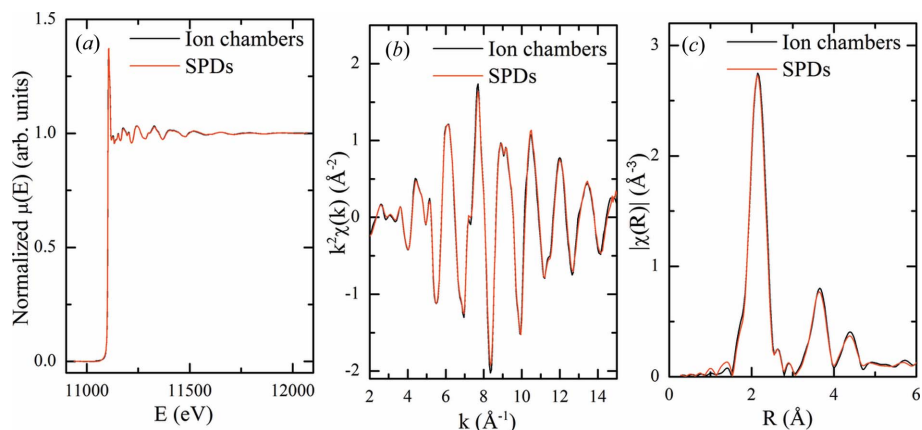


Figure 2 (a) Comparison of normalized Ge *K*-edge XAFS spectra of polycrystalline Ge powder measured in transmission mode using ion chambers and transmission Si photodiodes. (b) EXAFS $k^2\chi(k)$ functions and (c) Fourier transform magnitudes in the k -range 2.5–14.4 \AA^{-1} .

single-crystal DAC without compression at four different DAC orientations relative to the incident X-ray beam direction, as shown in Fig. 3. An XAFS spectrum of taped Ge powder is included for comparison. One can see obviously that there are just one or two broadened and weak DAC glitches in the full energy range of spectra *B*, *C* and *D* up to 800 eV above the absorption edge, showing that the number and intensity of Bragg glitches are remarkably suppressed by the introduction of the PHL as compared with normal methods (Hong *et al.*, 2009). Despite the comparable intensities of broadened Bragg reflection glitches to EXAFS and XANES oscillations, their weak interferences are still disastrous to the accurate extraction of geometrical parameters in the following fitting process. It was reported that the method of adjusting DAC orientation in energy-scanning XAFS is only effective in the case when the number of DAC glitches is small (Ohsumi *et al.*, 1986; Hong *et al.*, 2009). Therefore, a considerable decrease in the

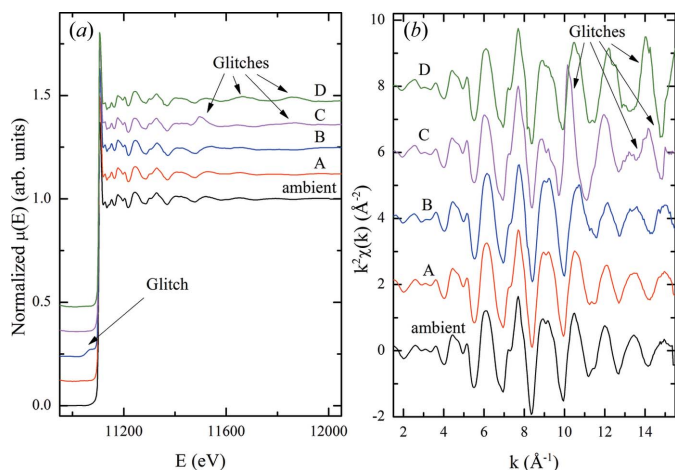


Figure 3 (a) Normalized Ge *K*-edge XAFS spectra of polycrystalline Ge powder collected at 2.0 GPa at four different DAC orientations *A*, *B*, *C*, *D*. The spectrum obtained at ambient pressure is also plotted for comparison. (b) EXAFS $k^2\chi(k)$ functions. The XAFS spectra *B* and *C* and the EXAFS $k^2\chi(k)$ functions show serious glitches owing to Bragg diffraction by single-crystal diamond anvils.

number of DAC glitches brings about an opportunity to remove completely the Bragg reflection glitches in a given energy range by rotating the DAC with respect to the X-ray beam. Further rotation of the DAC is carried out. After several adjustments of the DAC orientation, all the Bragg glitches are unexpectedly eliminated as demonstrated by the spectrum *A* in Fig. 3(a). Spectrum *A* is completely consistent with that of the taped Ge powder as confirmed in the k -space (Fig. 3b), proving that our method is effective in eliminating DAC glitches and one can easily obtain a high-quality XAFS spectrum with large enough glitch-free energy range.

A brief explanation of the suppression mechanism of the PHL on diamond glitches is proposed as follows. X-ray diffraction of single-crystal diamond only occurs for that part of the X-ray beam that is incident at the correct angle for the selected X-ray energy according to Bragg's law (Cullity, 1978),

$$2d \sin(\theta) = n\lambda = nhc/E, \quad (1)$$

where d is the crystal plane spacing, θ is the angle between the X-ray beam and the crystal surface, n is an integer, λ is the wavelength of the X-rays, h is Planck's constant, c is the speed of light, and E is the X-ray energy. The PHL consists of a bundle of hollow glass tubes shaped to collect and redirect the X-ray emission into a focus beam, and makes a large divergence for the output X-ray beam. The central fraction of the exit beam is small, but its intensity is the highest and the collimation is quite good. The central part goes straight to the diamond crystal, thereby making more efficient diffraction. The other part of the exit beam is large and its divergence increases gradually from the center to the edge, up to 15 mrad. For the divergent-beam X-ray diffraction of single-crystal diamond, the diffracted intensity is low because only a small fraction of the incident beam is at the correct energy and the correct angle. This results in the breaking of the Bragg diffraction condition for the largely diverged beam and significant weakening of the diamond glitches relative to the case without the PHL. Differentiating equation (1) gives the relation between divergent angle $\Delta\theta$ and energy spread ΔE ,

$$\cot(\theta)\Delta\theta = \Delta E/E. \quad (2)$$

As expressed by equation (2), we find that larger angular divergence will lead to larger energy spread and much more broadening for diamond glitches, compared with those reported using normal methods (Hong *et al.*, 2009). The intensity of many broadened diamond glitches is so weak that it could be safely ignored compared with EXAFS oscillations, consistent with the substantial reduction in the number of diamond glitches in Fig. 3(a). We note that the intensity of the central part of the focused X-ray beam is much stronger than that of the outer part, resulting in the incomplete elimination

capability of diamond glitches by the PHL. This might explain why, although the divergence of the incident X-ray beam is very large, one or two DAC glitches are still left, as shown in Fig. 3.

Our method is applied to investigate the high-pressure phase transition behavior of polycrystalline Ge powder using single-crystal DACs. Figs. 4(a) and 4(b) show Ge *K*-edge *in situ* EXAFS functions $k^2\chi(k)$ in the k -range 2.5–14 \AA^{-1} under compression and the magnitudes of their corresponding Fourier transform, respectively. The EXAFS functions $k^2\chi(k)$, as shown in Fig. 4(a), exhibit remarkable changes with the increase of pressure up to 23.7 GPa. Significant modification of the $k^2\chi(k)$ oscillation at 11 GPa was observed, indicating a structural transition from a cubic diamond type phase to a tetragonal β -Sn type phase (Olijnyk *et al.*, 1984; Menoni *et al.*, 1986; Di Cicco *et al.*, 2003; Mujica *et al.*, 2003; Baldini *et al.*, 2011). Corresponding changes can also be identified in the R -space of Fourier transform curves as shown in Fig. 4(b). The profiles of the cubic diamond type phase in R -space are characterized by three distinct peaks: one at 2.12 \AA represents the single-scattering contributions from the Ge–Ge first coordination shell, and the other two at 3.62 and 4.33 \AA are derived mainly from the single scattering of the second and third coordination shells, respectively. By compression to

11 GPa, the first peak at 2.12 \AA splits into two peaks located at 1.93 and 2.39 \AA , implying the coexistence of diamond type and β -Sn type phases at this pressure. This is associated with large structural disorder as shown by the significant decrease in intensity of the first peak. After 16.0 GPa, the two Ge–Ge split peaks merge into a single peak at 2.24 \AA , meaning that the diamond type phase has transformed completely to the β -Sn type phase. Further compression just leads to the bond distance contraction of the Ge–Ge first coordination shell, consistent with previous studies (Menoni *et al.*, 1986; Baldini *et al.*, 2011).

Although the present approach is focused on high-pressure XAFS with a DAC, the proposed method should be applicable to other similar situations as well. For example, a great deal of low-dimensional nanomaterials, such as nanoparticles, nanowire and film, are fabricated on a single-crystal substrate (silicon or sapphire) for the purpose of fundamental study and applications. The local structure related to these low-dimensional nanomaterials on single-crystal substrates is explored *via* XAFS in fluorescence or total-electron-yield mode because the sample of low-dimensional nanomaterial usually roots in a thin layer on the single-crystal substrate. However, several Bragg reflection glitches from the single-crystal substrate are usually riding on the XAS spectrum and destroy the collected data, resulting in a poor signal-to-noise XAFS spectrum. Although adjusting slightly the incident angle of the X-rays *via* turning the sample can sometimes avoid the Bragg reflection glitches, it is quite tricky and rather time-consuming. Overcoming the serious interference of these Bragg reflection glitches is essential of XAFS measurements for a large class of low-dimensional nanomaterials, yet an effective method to obtain an accurate XAFS spectrum free from glitches induced by the single-crystal substrate has been lacking. Similar to the case of high-pressure XAFS with a DAC, our PHL optics can also be employed to measure an XAFS spectrum in fluorescence or total-electron-yield mode for samples with a single-crystal substrate.

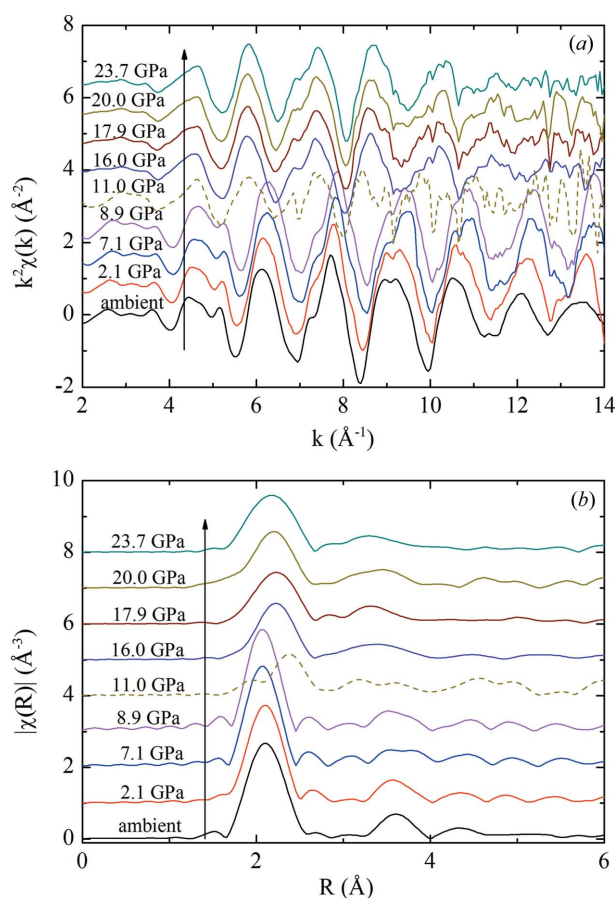


Figure 4
(a) Evolution of the EXAFS $k^2\chi(k)$ functions in the 2.5–14 \AA^{-1} k -range with pressure up to 23.7 GPa at selected pressures. (b) Magnitudes of the Fourier transforms of EXAFS spectra over the 0–6 \AA R -range at selected pressures.

4. Conclusion

We have performed the first high-pressure XAFS experiment of germanium with a single-crystal DAC using PHL re-focusing optics. The results demonstrate the capability of PHL optics in avoiding the Bragg glitches from single-crystal diamonds for high-pressure XAFS experiments with DACs. Our method significantly facilitates high-pressure XAFS experiments with DACs because a large divergence induced by PHL leads the DAC glitches to be strongly suppressed, whereas the XAFS spectrum cannot be affected by the divergence. Although the DAC glitches are not able to be eliminated completely by the PHL after a brief attempt, most of them are efficiently suppressed. A considerable reduction in the number of glitches provides an opportunity to remove easily the remaining glitches by rotating the DAC by a few degrees with respect to the X-ray beam. The example displays that the quality of the collected Ge *K*-edge high-pressure XAFS spectra of polycrystalline Ge powder with an increase

of pressure up to 23.7 GPa appears comparable with those obtained outside the DAC. This approach opens up the possibility to perform a more detailed quantitative analysis of high-pressure EXAFS data with full pressure/temperature capability of a DAC (300 GPa/5000 K).

The authors sincerely thank the staff of the high-pressure station of BSRF for pressure calibration. This work is financially supported by the National Natural Science Foundation of China (Grant No. 10979060 and 11179010).

References

- Baldini, M., Aquilanti, G., Mao, H.-k., Yang, W., Shen, G., Pascarelli, S. & Mao, W. L. (2010). *Phys. Rev. B*, **81**, 024201.
- Baldini, M., Yang, W., Aquilanti, G., Zhang, L., Ding, Y., Pascarelli, S. & Mao, W. L. (2011). *Phys. Rev. B*, **84**, 014111.
- Bunker, G. (2010). *Introduction to XAFS*. Cambridge University Press.
- Cullity, B. D. (1978). *Elements of X-ray Diffraction*, 2nd ed. London: Addison-Wesley.
- Di Cicco, A., Frasini, A. C., Minicucci, M., Principi, E., Itié, J. & Munsch, P. (2003). *Phys. Status Solidi B*, **240**, 19–28.
- Hong, X., Newville, M., Prakapenka, V. B., Rivers, M. L. & Sutton, S. R. (2009). *Rev. Sci. Instrum.* **80**, 073908.
- Itié, J. P., Baudalet, F., Congeduti, A., Couzinet, B., Farges, F. & Polian, A. (2005). *J. Phys. Condens. Matter*, **17**, S883–S888.
- Itie, J.-P., Baudalet, F., Dartyge, E., Fontaine, A., Tolentino, H. & San Miguel, A. (1992). *High Pres. Res.* **8**, 697.
- Jayaraman, A. (1983). *Rev. Mod. Phys.* **55**, 65–108.
- Katayama, Y., Mezouar, M., Itie, J. P., Besson, J. M., Syfosse, G., Le Fevre, P. & Di Cicco, A. (1997). *J. Phys. IV Fr.* **7**, 1011–1012.
- Katayama, Y., Tsuji, K., Shimomura, O. & Oyanagi, H. (1996). *J. Non-Cryst. Solids*, **205–207**, 199–202.
- Koningsberger, D. & Prins, R. (1987). *X-ray Absorption: Principles, Applications, Techniques of EXAFS, SEXAFS and XANES*. New York: John Wiley and Sons.
- Krumrey, M., Gerlach, M., Hoffmann, M. & Müller, P. (2007). *AIP Conf. Proc.* **879**, 1145–1147.
- Menoni, C., Hu, J. & Spain, I. (1986). *Phys. Rev. B*, **34**, 362–368.
- Mujica, A., Rubio, A., Munoz, A. & Needs, R. J. (2003). *Rev. Mod. Phys.* **75**, 863–912.
- Ohsumi, K., Sueno, S., Nakai, I., Imafuku, M., Morikawa, H., Kimata, M., Nomura, M. & Shimomura, O. (1986). *J. Phys. Colloq.* **47**, C8-189–C8-192.
- Olijnyk, H., Sikka, S. & Holzapfel, W. (1984). *Phys. Lett. A*, **103**, 137–140.
- Pascarelli, S., Mathon, O. & Aquilanti, G. (2004). *J. Alloys Compd.* **362**, 33–40.
- Petitgirard, S., Borchert, M., Andrault, D., Appel, K., Mezouar, M. & Liermann, H. P. (2012). *Rev. Sci. Instrum.* **83**, 013904.
- Proost, K., Vincze, L., Janssens, K., Gao, N., Bulska, E., Schreiner, M. & Falkenberg, G. (2003). *X-ray Spectrom.* **32**, 215–222.
- Ravel, B. & Newville, M. (2005). *J. Synchrotron Rad.* **12**, 537–541.
- Sapelkin, A. V., Bayliss, S. C., Russell, D., Clark, S. M. & Dent, A. (2000). *J. Synchrotron Rad.* **7**, 257–261.
- Schmidt, C., Rickers, K., Wirth, R., Nasdala, L. & Hanchar, J. (2006). *Am. Mineral.* **91**, 1211–1215.
- Silversmit, G., Vekemans, B., Nikitenko, S., Bras, W., Czech, V., Zaray, G., Szaloki, I. & Vincze, L. (2009). *J. Synchrotron Rad.* **16**, 237–246.
- Tamura, K., Hosokawa, S., Inui, M., Yao, M., Endo, H. & Hoshino, H. (1992). *J. Non-Cryst. Solids*, **150**, 351–355.
- Tolbert, S. H. & Alivisatos, A. P. (1995). *Annu. Rev. Phys. Chem.* **46**, 595–626.
- Vanpeteghem, C., Nelmes, R., Allan, D., McMahon, M., Sapelkin, A. & Bayliss, S. (2001). *Phys. Status Solidi B*, **223**, 405–409.
- Vincze, L., Wei, F., Proost, K., Vekemans, B., Janssens, K., He, Y., Yan, Y. & Falkenberg, G. (2002). *J. Anal. At. Spectrom.* **17**, 177–182.
- Wilke, M., Appel, K., Vincze, L., Schmidt, C., Borchert, M. & Pascarelli, S. (2010). *J. Synchrotron Rad.* **17**, 669–675.